Applied Ocean Research

Airgap analysis of floating structures: first- and second-order transfer functions from system identification

Bert Sweetman*, Steven R. Winterstein, C. Allin Cornell

Department of Civil and Environmental Engineering, Stanford University, California 94305-4020, USA

Abstract

System identification is used in a detailed comparison of model test data and numerical diffraction results. 'Optimal' quadratic transfer functions based on system identification of measured data are compared with those resulting from WAMIT hydrodynamic analysis and those from Stokes theory in order to understand the implications of a previously proposed 'Stokes substitution', which applies a hybrid of second-order transfer functions resulting from hydrodynamic diffraction and those resulting from Stokes wave theory. The goodness-of-fit of a second-order model, i.e. fraction of power explained through a second-order system identification, is examined to assess the possibility that a higher-order model may be needed. The results of the system identification suggest that (a) the Stokes substitution is reasonable and (b) quadratic transfer functions at high frequencies resulting from WAMIT analysis are not reasonable. © 2002 Elsevier Science Ltd. All rights reserved.

Keywords: Airgap; Quadratic transfer functions; WAMIT post-processing; Model test data analysis; Hydrodynamic analysis

1. Introduction and background

Airgap modeling is of concern for both fixed and floating structures, but it is particularly challenging in the case of floating structures because of their large volumes and the resulting effects of wave diffraction and radiation. Numerical hydrodynamic diffraction analysis and physical model tests are commonly used to study wave–structure interaction as part of the design process. If model tests are to be performed, diffraction calculations are still needed to determine the locations at which airgap probes should be placed on the model.

Standard airgap response prediction uses linear theory, which generally does not effectively reproduce measurements from model tests [1–4]. First-order diffraction is often selected over the more powerful second-order because of its relative simplicity, ease of use and robustness of the solution. While second-order diffraction effects are expected to better reflect observed data, these radiation/diffraction panel calculations have been found sometimes to over-predict airgap demand [2,5,6].

In Refs. [5,6], the numerical impact of modeling second-order diffraction effects was assessed by comparing various predictions of the statistical behavior of the free surface at the nine airgap probe locations shown in Fig. 1. Full second-order hydrodynamic and statistical theory was applied and a new method was proposed in which quadratic transfer functions (QTFs) associated with long-periods are provided by WAMIT results, while those associated with shorter periods are derived from Stokes wave theory.

This proposed use of QTFs predicted by Stokes theory for high frequencies is in apparent conflict with the theoretical recognition that Stokes theory and diffraction analysis results are expected to converge in the long wave limit, i.e. low frequencies. This apparent conflict helps to motivate the present work; one goal here is to quantify the impact of the Stokes substitution on predicted quadratic transfer functions as compared with those obtained from measured data or from diffraction analysis.

Here, quadratic transfer functions for the free surface elevation relative to a fixed observer are examined more closely, as is the Stokes substitution proposed in Refs. [5,6]. Second-order transfer functions are derived by examining model test data in the inverse order: trying to predict the first- and second-order airgap demand response transfer functions based exclusively on observed airgap demand response to a known sea-state. The results of this system

* Corresponding author. Tel.: +1-650-725-0360; fax: +1-650-725-9755.
E-mail addresses: bert.sweetman@stanfordalumni.org (B. Sweetman), steven.winterstein@stanford.edu (S.R. Winterstein), cornell@cive.stanford.edu (C.A. Cornell).
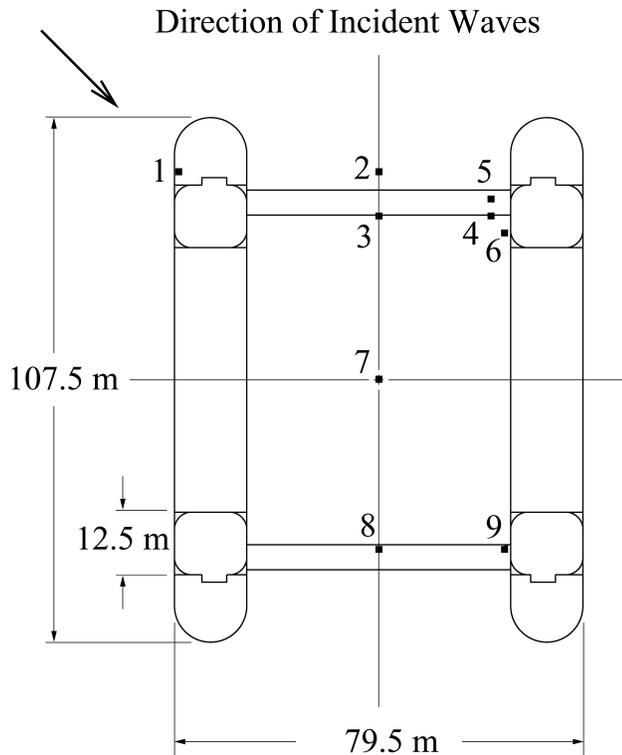
Fig. 1. Plan view of Veslefrikk platform and location of airgap probes.

Fig. 2. Airgap variable definitions.

identification are compared with results of WAMIT [7] hydrodynamic diffraction analysis, Stokes wave theory, and a hybrid between these two.

2. Airgap notation and the Veslefrikk model

As in Refs. [5,6], hydrodynamic diffraction results come from WAMIT 5.3 [7], a second-order panel diffraction program. Model test data come from a 1:45 length-scale model of Veslefrikk and are used for verification of the hydrodynamic analysis. The model tests were performed in the wave tank at Marintek using various types of irregular waves [8]. All analysis and model test results presented here are relevant to the Veslefrikk semi-submersible. Analysis here applies to long-crested waves traveling along the diagonal of the structure. Other relevant particulars for Veslefrikk as analyzed include: draft: 23 m, displacement: 40 692 ton, airgap to still water level: 17.5 m and water depth on location: 175 m.

As shown in Fig. 2, the airgap, $a(t)$, can be considered a linear combination of three terms: a_0, the still-water airgap distance, $\eta(t)$, the wave surface elevation at a particular location along the structure measured with respect to a fixed observer, and $\delta(t)$ the corresponding vertical motion of the platform. Modeling attention is focused here on $\eta(t)$. $\eta(t)$ is assumed to be a sum of incident and diffracted waves, η_i and η_d, each of which is a sum of first- and second-order components.

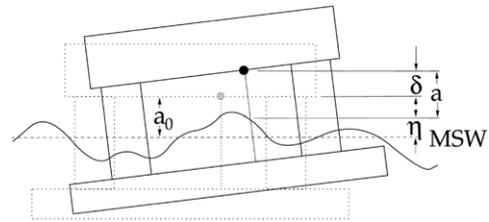The relative airgap at each of the wave-probe locations

and the platform rigid-body motions have been recorded. The rigid body motions permit estimation of the net vertical displacement, $\delta(t)$, at any field-point location (x, y). This estimate is then subtracted from the measured airgap to determine the absolute wave elevation, $\eta(t)$, with respect to a fixed observer. In Refs. [5,6], the resulting $\eta(t)$ was used for comparison with analytical predictions. Here, the resulting $\eta(t)$ is used as a basis to identify those transfer functions resulting from the structure's effect on the wave profile. The resulting 'observed' transfer functions can then be compared directly with corresponding transfer functions predicted by hydrodynamic diffraction theory for a fixed structure.

3. Prior work and key results

Key results from Refs. [5,6] help to motivate the work presented in this paper, so some results and discussion from Refs. [5,6] are repeated here. These results are summarized for two sea-states in Fig. 3, which compares the standard deviation of the observed airgap demand (η) process and measured peaks to predicted values. These predictions are based on alternative methods of post-processing a single set of WAMIT hydrodynamic analysis results.

The methods of predicting these are described in more detail in Refs. [5,6]. The statistical moments are estimated using linear transfer functions (LTFs) and quadratic transfer functions (QTFs) in conjunction with a specified sea-state to directly predict the statistics of the airgap response. These statistical moments are calculated using the methods originated by Kac and Siegert [9] and later expanded by Næss [10,11]. Implementation of the theory is described in Ref. [12], with extensions to airgap analysis from Ref. [4].

The expected maximal peaks shown on the plot are calculated as follows: The expected maximum of a standard Gaussian process in N cycles is first determined [13]. The Hermite model is then applied [14] using the theoretical skewness and kurtosis estimates to transform this Gaussian maximum to predict the non-Gaussian extreme value. Results presented here use an optimization routine to minimize error in matching skewness and kurtosis values. These analytical results predict mean 3-hour maxima, which are compared in Fig. 3 with average maxima over five separate 3-hour model tests for the 12-meter bimodal
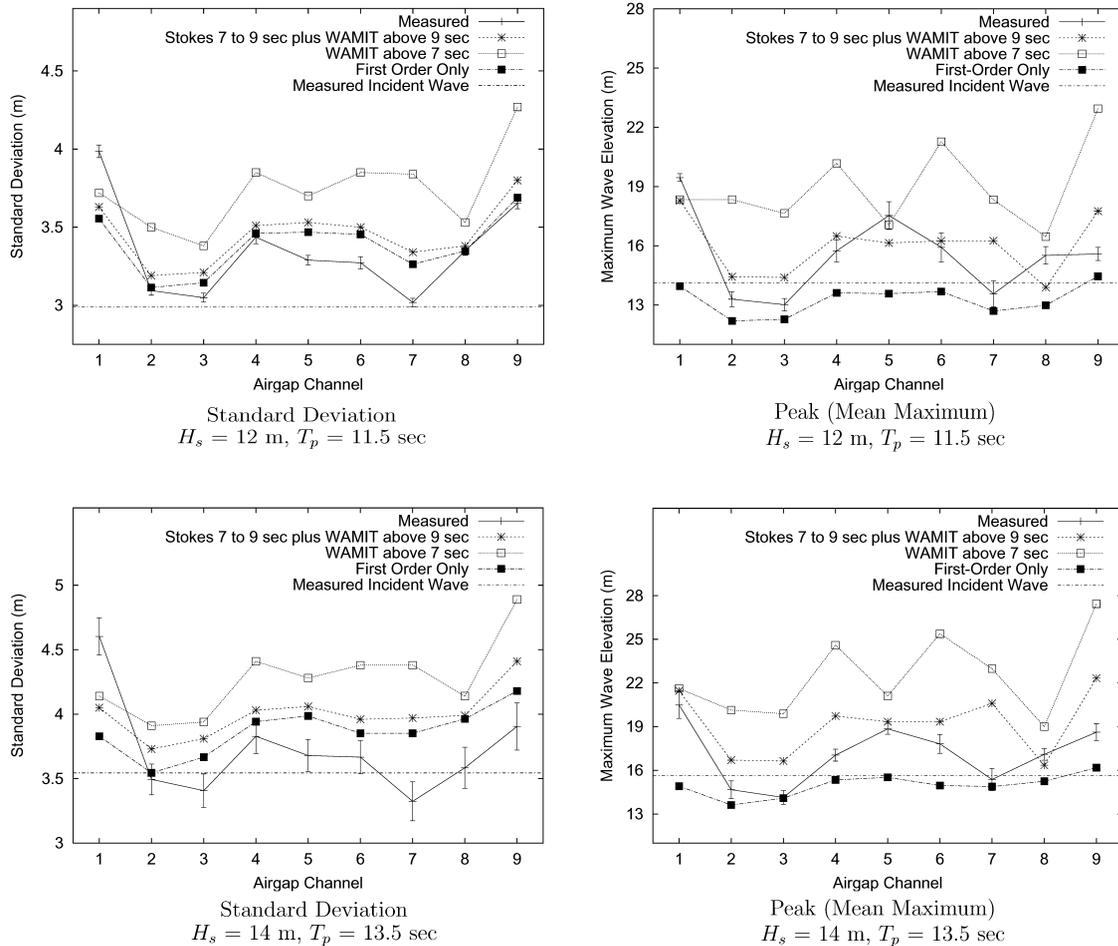
Fig. 3. Absolute wave elevation, η, with respect to a fixed observer: predictions compared with measured data. Error bars calculated as the standard deviation of the n observations divided by $\sqrt{n}$.

sea-state and six separate 3-hour tests for the 14-meter JONSWAP sea-state.

3.1. Key results

WAMIT QTFs have been observed to grow exceedingly large for low periods [2,5] and as shown later in Figs. 11 and 13. In these WAMIT analyses, a convergence analysis did not indicate a convergence problem, and mesh density was not observed to significantly affect results. Use of the resulting QTF values, however, lead to the substantial over-prediction of the response in Fig. 3. It was hypothesized that more accurate prediction results can be obtained by using the WAMIT QTFs only over the range for which they appear reasonable: in this case, periods greater than 9 s. Fortunately, the peak of the input wave spectrum is well within this period range for these model tests.

A Stokes substitution is proposed in Refs. [5,6]. In this method, a QTF predicted by Stokes theory is substituted for that predicted by WAMIT if the average of the frequency pair, $(1/2)(f_1 + f_2)$, is greater than a cut-off frequency, $f_c = 1/T_c$. Applying the Stokes substitution with $T_c = 9$ s results in the line denoted 'Stokes 7–9 s plus WAMIT above 9 s' in

Fig. 3. The large over-prediction in 'WAMIT above 7 s', relative to both the Stokes substitution with $T_c = 9$ s and to measured data, confirms that the WAMIT results should not be trusted for periods as low as 7 s.

The proposed Stokes substitution is believed to be better than the three obvious alternatives: (1) use of the complete QTF matrix predicted by WAMIT has been found to yield unrealistic results, (2) simply zeroing-off the unused QTFs would be straight-forward, but the actual QTFs below T_c are believed to be non-zero, (3) somehow extrapolating those QTFs believed to be reasonable may be possible, but the details of a valid QTF extrapolation are elusive.

Considering standard deviation plots in Fig. 3, second-order diffraction has only a minor effect on the standard deviation, so it appears that linear diffraction alone may be sufficient to accurately predict the rms level of the wave elevation, and hence that of the airgap response. The non-Gaussian effects associated with increased values of the coefficients of skewness and kurtosis, however, substantially increase the prediction of the mean maximum from the 'first-order only' result to approximate that of the observed model test data ('measured'). Column run-up effects are expected to exhibit a non-linearity greater than quadratic;

the prediction ability of a quadratic model implies the model-test probes were positioned sufficiently far from the columns to avoid measurement of run-up effects.

The Stokes substitution appears to be the best predictor of mean-maxima shown in Fig. 3. Note that 'first-order only' generally under-predicts the observed mean-maxima, while use of all 'WAMIT above 7 s' generally over-predicts the observed data. The magnitude of the predicted peak using the Stokes substitution is more nearly centered amongst the measured data.

The simplicity and apparent success of the Stokes substitution proposed in Refs. [5,6] leads to the hope that it can be used in practical design applications in which second-order airgap effects are believed to be important. However, the success of the new method is at odds with the theoretical recognition that Stokes theory is only expected to converge in the long-wave limit; thus, a more careful examination of the second-order transfer functions and the proposed substitution is presented.

4. Black-box system identification

The objective of second-order system identification is to identify the first- and second-order transfer functions that best relate the observed input and response time-histories. The term 'black-box' refers to the fact that the system-identification method does not rely on any assumed physical properties of the system itself, i.e. the identification algorithms employed are applicable to any dynamic system which has, or is suspected to have, first- and second-order transfer functions. The schematic input and output of the process applied here are shown in Fig. 4. The 'goodness of fit' shown on the lower right will be discussed later. The numerical algorithm employed is that developed by Ude [15].
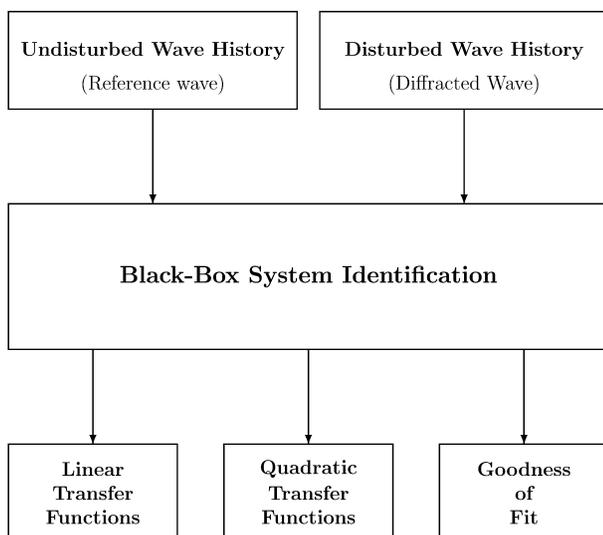

Fig. 4. System ID input and output.

It was implicitly assumed in Refs. [5,6] that the poorly behaved QTFs were not correct. One possibility, though, is that these QTFs are correct to second-order; and that the problem lies in the second-order assumption. Under this hypothesis, it could be that inclusion of higher-order terms (e.g. third, fourth, etc.) would have an offsetting effect resulting in prediction of a total process which agrees well with observed data. It should be noted that like most hydrodynamic wave theories, diffraction theory is based on a perturbation expansion, application of such an expansion relies on the assumption that higher-order terms are smaller than lower-order terms: an assumption which would seem to be violated by the subject hypothesis.

Ignoring the possible misuse of perturbation theory, if the hypothesis that higher-order terms are needed is correct, then:

- the identified quadratic transfer functions should closely match those predicted by WAMIT;
- there should be a large amount of power in the time-histories that could not be explained by best-fitting quadratic transfer functions (i.e. higher-order terms should be needed to explain this power).

This hypothesis is tested by application of system identification to observed time-histories. The goal is to compare identified transfer functions with those predicted by WAMIT and by Stokes second-order theory. WAMIT and Stokes are already known to be in strong disagreement for high-frequency terms, so assessment of the amount of power in the histories which cannot be explained by best-fitting linear transfer functions and quadratic transfer functions (LTFs and QTFs) can be used to gain additional insight into the system behavior and the need for still higher-order non-linear effects.

In order to make such an assessment, it is first critical to assess the capability of extracting meaningful LTFs and QTFs by black-box system identification. To assess the capability to extract meaningful LTFs and QTFs, first, a synthetic data set is generated which matches an existing measured data set: 6×3-hour realizations of the $H_s = 14$ m, $T_p = 13.5$ s JONSWAP sea-state. The sea-states are simulated using the target power spectrum and truncated WAMIT transfer functions. Note that the accuracy of the WAMIT results is not tested in this calculation: only the capabilities of simulation and system identification. The aim is to verify that the system identification algorithm is capable of recovering a reasonable approximation of the WAMIT results from simulated data based on use of these results.

Table 1 shows a summary of the legend for results of identifying linear transfer functions from the simulated wave time-histories for wave probes located at the platform center and up-stream of the first column (Figs. 5–8).

Table 1
Cases considered in system ID examples (summary of legend for system ID cases)

WAMIT. Transfer functions as predicted by diffraction analysis
Simulated. WAMIT transfer functions are used in *TFPoP* to simulate an η time-history. The resulting time-history is then 'identified' to (hopefully) recover the WAMIT transfer functions
Observed history. Transfer functions are identified from observed histories of η and measured reference wave (wave 2)
Translated history. The reference wave (wave 2) is first numerically 'translated' to approximate the incident wave history as it would have been observed from a wave probe fixed to the moving vessel (in absence of the vessel). Transfer functions are then identified from observed histories of η and the translated reference wave

---

4.1. Linear transfer functions from system identification: simulated data

System identification of simulated data should be particularly effective because the simulated data results from a true second-order system. It is generated using only first- and second-order transfer functions and first- and second-order theory. There is no opportunity for introduction of higher-order effects into the time-history. Time-histories resulting from this second-order system are next identified using second-order system identification. Failure to regenerate reasonable approximations of the input transfer functions would be unexpected. All of the WAMIT LTF results used to generate the time-histories are shown in the plots.

Figs. 5 and 6 demonstrate the effectiveness of the system identification algorithm. Good agreement in both magnitude and phase is observed between 'WAMIT LTFs' and 'simulated' for both locations 1 and 7. Considering the platform center (Fig. 5): the mean offset from the reference wave location is very small, so as expected, the figures show relative phase to be very near zero for both the WAMIT and simulated results.

The phase of the linear transfer function at the location forward of the first column is shown in Fig. 6. Here, the phase is non-zero, and the phase rate of change progressively increases with decreasing period, as expected. This phase-change is discussed in more detail in Section 4.2.

4.2. Linear transfer functions from system identification: measured data

Having attained success with simulated time-histories, measured data are next considered. Figs. 7 and 8 are equivalent to Figs. 5 and 6 except that measured data are now applied. Input to the identified system is η_i, the undisturbed incident wave, which is the measured reference wave. The output process is η, the diffracted wave as recreated from measured records of airgap and vessel motions, i.e. $\eta_d = \eta_d + \eta_i$. The error bars, $\hat{\sigma}$, are calculated as

$$\hat{\sigma} = \sqrt{\text{RSS}/(n - p - 1)} \qquad (1)$$

where RSS is the residual sum of squared errors in the linear regression used in the identification process (Section 5), n is the number of observations in the regression (the number of segments into which the original time-history was cut) and p is the number of predictors in the regression (one in this case because a zero-intercept was specified in the regression) [15]. Here, the 18 h of data for the $H_s = 14$ m sea-state is divided into $n = 322$ segments of 598 time-points.

As can be seen in the figures, the LTFs are consistent in overall trends, but diverge somewhat in magnitude, particularly at location 7 (platform center), where the magnitudes typically differ by about 25%. It is expected that transfer functions estimated from data are of higher quality than those provided by diffraction analysis. In the case of location 7, the transfer functions produced by WAMIT can be observed to be excessively high by simple comparison of the standard deviation of the incident wave (3.5 m) with that of the diffracted wave (3.3 m). It is clear that the transfer functions should be less than 1, while the WAMIT transfer functions are generally greater than 1.

The final segment of data shown in the plot is denoted 'translated history'. This result is produced by manipulating the measured reference wave (wave 2) such that it approximates the incident wave history as it would have been observed from a wave probe fixed to the moving vessel (in absence of the vessel) [16,17]. Wave mechanics are assumed to be second-order in the translation process, though the motion of the vessel in the basin is not.

The phases are also shown in Figs. 7 and 8. First considering the platform center (Fig. 7): the mean offset from the reference wave location is very small, which results in near-zero relative phase for the WAMIT results. The 'measured' and 'translated' results should also be very near zero. Some divergence from zero is found for low periods.

Low period waves are physically shorter than high period waves[1] so small horizontal differences correspond to relatively larger phase differences for decreasing periods. Some divergence from zero is expected for the 'observed' case because the center of the platform is moving throughout the measurement process. This horizontal movement corresponds to a phase shift.

More dramatic phase effects can be seen at the location up-stream of the first column (Fig. 8). Here, the phase is, as expected, non-zero for identification of the 'observed', and 'WAMIT' histories. The translation procedure is intended to make the phase near zero. The 'translated' result is observed to be more nearer to zero phase than the 'observed' result, but there is still non-zero phase for short-period waves. Again, relative phase effects are magnified for short-period waves.

---

[1] Linear theory yields $L = gT^2/(2\pi)$, where L is wavelength, g is acceleration due to gravity, and T is wave period.
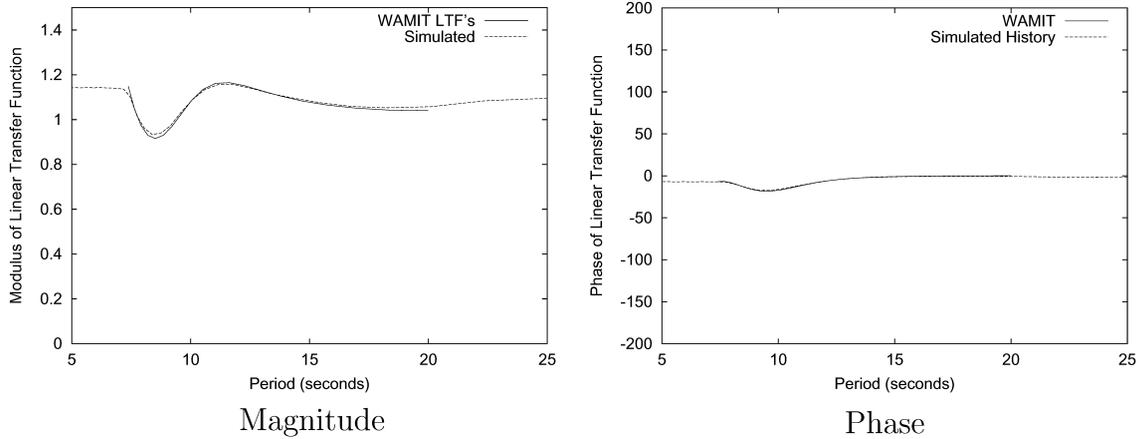
Fig. 5. System ID effectiveness: η LTF modulus and phase for location 7—platform center; $H_s = 14.0$ m, $T_p = 13.5$ s.

The 'translated' result is again expected to show zero-phase, and again shows some divergence from zero. The translation at location 1 consists of a relatively long fixed spatial shift (the fixed distance between the locations of the wave probes on the model) plus the smaller dynamic shift (horizontal movement of the vessel). The phase rate of change progressively increases with decreasing period, as expected because these shorter wavelengths are smaller relative to the fixed spatial shift.

All results presented in Figs. 7 and 8 are for a single sea-state: A JONSWAP wave spectrum with a 14 m significant wave height and a 13.5 s peak period. A transfer function is, by definition, a property of the structure and so should be independent of the environmental parameters. Another test of the adequacy of first- and second-order models, and of the system identification process, is to verify that the resulting transfer functions are in fact independent of environment.

Fig. 9 compares transfer functions identified from a sea-state corresponding to an $H_s = 14$ m, $T_p = 13.5$ s JONSWAP spectrum with those corresponding to an $H_s = 12$ m, $T_p = 11.5$ s bimodal spectrum. Both of the figures show reasonably good agreement, suggesting that these estimates

of the linear transfer functions are in fact reasonably independent of the sea-state.

4.3. Quadratic transfer functions from system identification

Figs. 10–13 show the on-diagonal results of identifying the quadratic transfer functions from the observed time-histories. Also shown in these figures are the QTFs resulting from a WAMIT hydrodynamic analysis and the theoretical Stokes second-order result.

First, the effectiveness of the simulation and system identification is considered. As in the linear case (Section 4.1), WAMIT transfer functions are used to simulate an η time-history; the resulting time-history is then identified to (hopefully) recover the WAMIT transfer functions. Fig. 10 shows a comparison between the input transfer functions predicted by WAMIT, and those resulting from the system identification of a simulated time-history. The ability to recover the input quadratic transfer functions is not as pronounced as in the linear transfer function case. This may be due to the finite length of the generated time-history on which the identification is performed. Note that there were no QTFs specified above a 20 s period. The divergence of
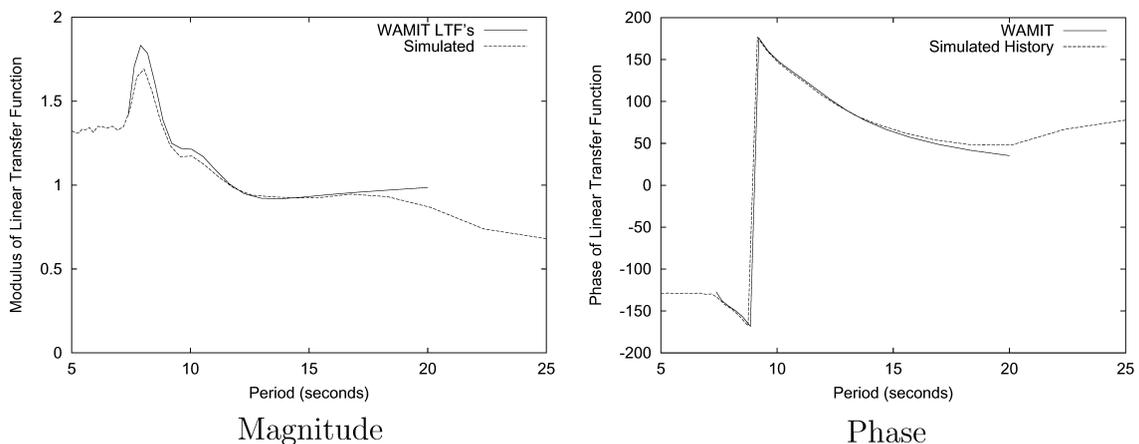

Fig. 6. System ID effectiveness: η LTF modulus and phase at location 1—forward of first column; $H_s = 14.0$ m, $T_p = 13.5$ s.
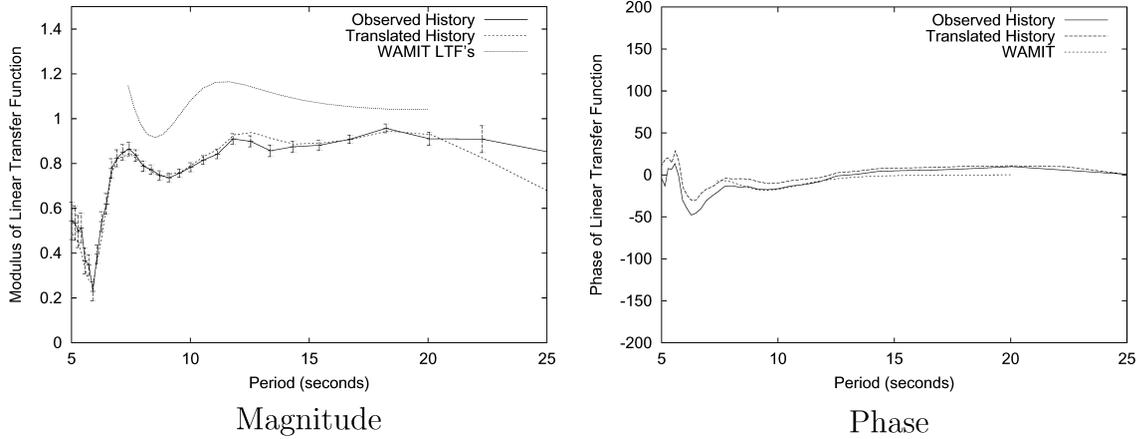
Fig. 7. System ID results: η LTF modulus and phase for location 7—platform center; $H_s = 14.0$ m, $T_p = 13.5$ s.

identified QTFs at long periods are discussed in conjunction with Figs. 13 and 17.

Fig. 13 shows a comparison between the quadratic transfer functions identified from the observed time-histories and those predicted by WAMIT and Stokes theory. It can be observed that the WAMIT result diverges from the system ID result for periods less than about 8 s. The identified QTFs follow the Stokes theoretical estimate far more closely than they do the results of WAMIT. This result supports the reasonableness of the Stokes substitution proposed in Refs. [5,6]. Unfortunately, the identified QTFs diverge from both theory and WAMIT results in the long period ranges.

Fig. 13 shows the same data as Fig. 12, but a linear vertical scale is applied, error-bars are shown, and WAMIT and Stokes results are included. The error bars are the $\hat{\sigma}$ calculated in Eq. (1). The error bars at the low-period range are considerably larger than those in the part of the spectrum in which there is substantial wave energy, but not nearly as large as those for periods above 20 s. Larger error bars are expected at high and low periods because there is less wave energy to be identified far from the spectral peak.

The much larger error bars at the long periods are probably because interactions between long (e.g. 25 s) wave cycles are sought, which considerably increases the data demands. There are fewer 25-second wave cycles in a wave record of fixed duration than there are 5-second cycles. The recurrence of this systematic over-prediction in the long-period range suggests there is some systematic bias in the identification process for this range.

As in the case of linear transfer functions, quadratic transfer functions should also be independent of the sea-state. Fig. 12 is the quadratic equivalent of Fig. 9; it verifies that the identified QTFs are reasonably independent of sea-state. The divergence at long periods is again most probably due to lack of long-period data in the time-histories and low amplitudes in those few long period wave cycles that are available. Again, this agreement supports the adequacy of a second-order model of the wave elevation surface, and the lack of significant higher-order effects.

5. Goodness of fit

The third and final piece of output produced by the system identification routine is the goodness of fit. What this
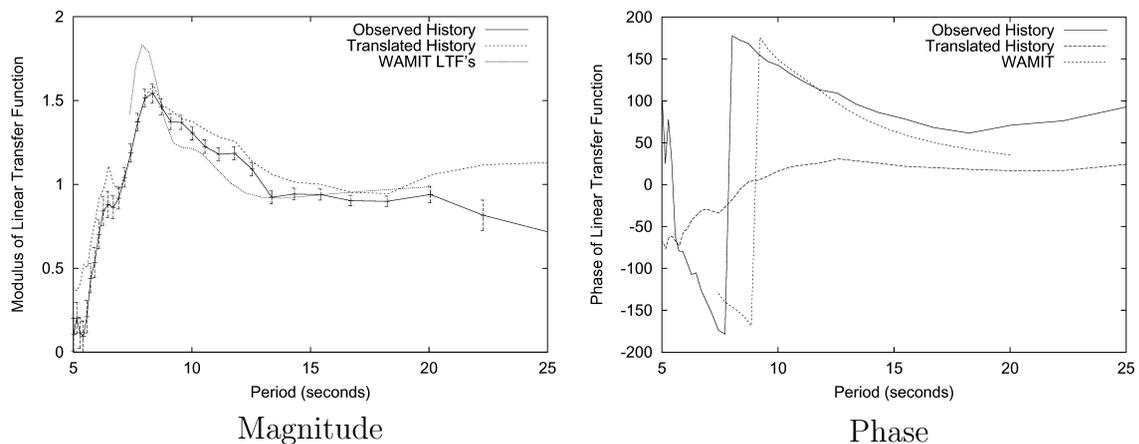

Fig. 8. System ID results: η LTF modulus and phase at location 1—forward of first column; $H_s = 14.0$ m, $T_p = 13.5$ s.
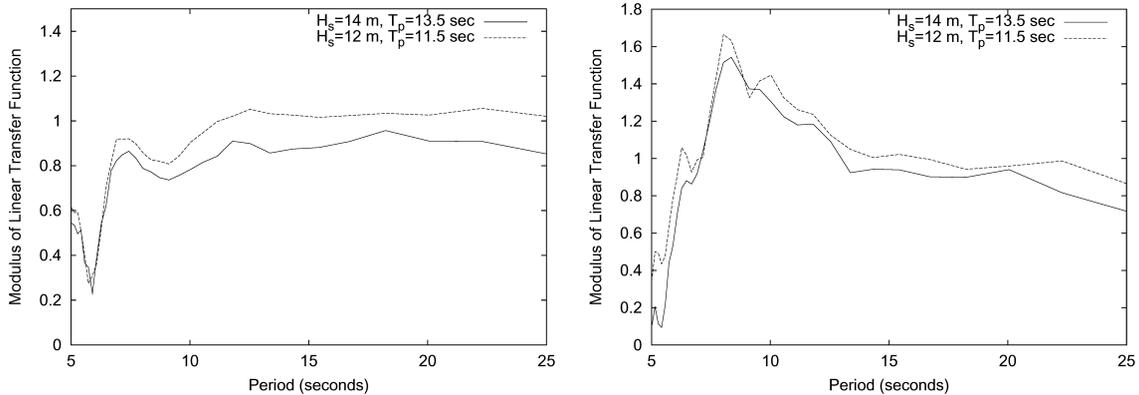
Fig. 9. System ID results: η LTFs; locations 7 (left) and 1 (right): platform center and in front of first column.

output measures is how well the empirically derived transfer functions explain the energy observed in the wave time-history at each frequency used in the analysis. To explain the derivation of this quantity an explanation about the method developed by Ude [15] is necessary. Without computational details, the key steps to the identification process, which lead to the estimate of goodness of fit are as follows:

(1) Long input time-histories are divided into a number of smaller segments. (In the analysis for the $H_s = 14$ m, $T_p = 13.5$ s sea-state, an 18-hour time-history is divided into 322 segments of 598 points, or about 200 s in the time-history.)

(2) An independent Fourier analysis is performed on each segment, resulting in a point-estimate of the transfer function for that segment (for each frequency).

(3) Linear regression is applied to these segment-specific point-estimates (for each frequency (LTF), or pair (QTF) to estimate the transfer function.

$$y = \beta x + \epsilon \qquad (2)$$

For the linear terms, the (x, y) pairs are the input and output at that frequency for each segment of the time-history, and β is the resulting point estimate of the

LTF. For the quadratic terms, each 'frequency' is actually a frequency pair, but the regression on the QTF remains linear for each frequency pair.

(4) The scatter about the regression line at each frequency (pair) is a measure of the goodness of fit. Zero scatter implies the transfer function explains 100% of the power; completely random scatter implies the transfer function explains none of the power.

5.1. Goodness of fit results

Fig. 14 also shows the total goodness of fit for locations 7 and 1, the platform center and up-stream of the first column, respectively. The horizontal line at 1.0 represents the theoretically perfect fit. The 'simulated history' is nearly as good as the theoretical optimum. The excellence of the fit is not surprising: the simulated history *is* a second-order process consisting of *only* first- and second-order input waves which are acted on by *only* first- and second-order hydrodynamic transfer functions (WAMIT) and therefore have only first- and second-order components in the time-history. Since the response is a second-order process, one would expect a second-order system identification to be capable of explaining essentially all of the energy in the system response.
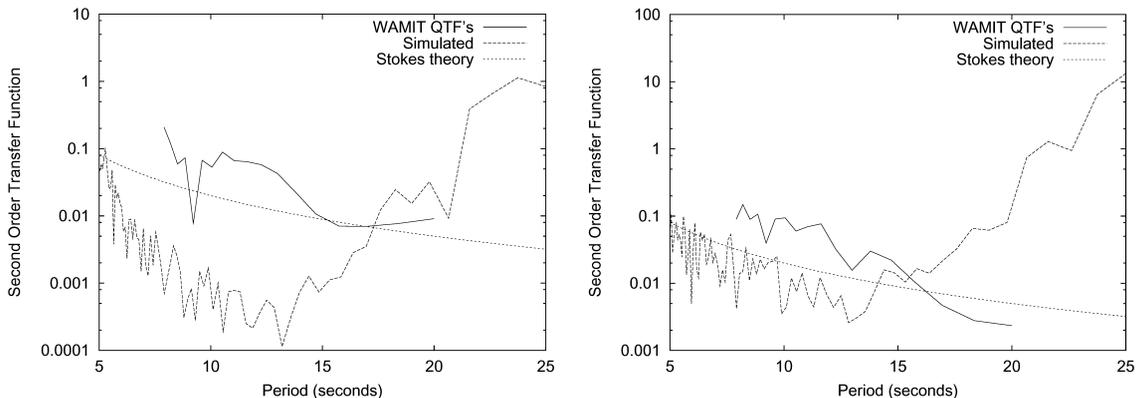

Fig. 10. ID effectiveness: η QTFs from identification of simulated data and from theory; location 7 (left) and 1 (right): platform center and in front of first column. $H_s = 14.0$ m, $T_p = 13.5$ s.
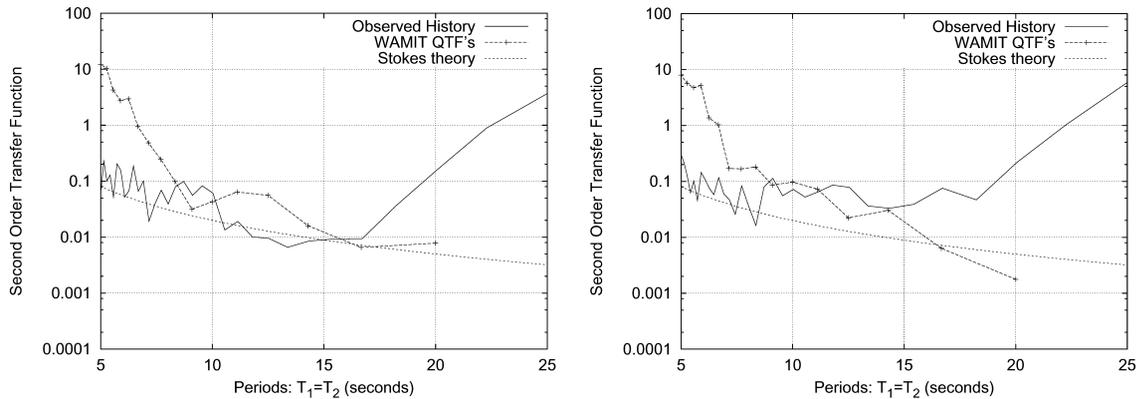
Fig. 11. System ID results: η QTFs from identification of observed data and from theory; location 7 (left) and 1 (right): platform center and in front of first column. $H_s = 14.0$ m, $T_p = 13.5$ s.

Next considering the 'observed' and 'translated' histories at location 7 of Fig. 14, it is observed that there is little change in the goodness of fit produced by the translation process. Also, the goodness of fit is quite good over the middle of the period range, spanning those frequencies containing most of the wave energy. Recall that the average location of wave probe 7 is very near that of the reference wave, so there is almost no rigid body shift in the translation. Thus, the translation is reflecting only the effects of vessel motion.

Fig. 14 also shows the total goodness of fit for location 1, up-stream of the first column. Again, the 'simulated' result shows considerably better goodness of fit than do results based on the measured time-histories. The simulated history is again a second-order system, so better fit of the simulated data than of the measured data is expected. Here, the simulation explicitly includes the transfer functions between the wave input at the reference location and the response at the wave probe location, but does not explicitly include those transfer functions which are implied by dispersion of the wave profile (i.e. the dispersion and second-order correction explicitly calculated in the translation process). Thus, the transfer functions sought through identification result from two physical processes: diffraction and dispersion. Apparently the increased complexity of the

problem has slightly decreased the ability of the system identification to fully explain the observed power.

Next considering the 'observed' and 'translated' histories at both locations in Fig. 14, it is observed that there is little change in the goodness of fit introduced by the translation process. Here, there is a significant rigid body shift between the reference wave location and the location of airgap probe 1. The improvement in prediction capability is almost entirely due to simplification of the problem by separating the identification into two steps. The largest effect in the translation is that of dispersing the incident wave process as a second-order system. Thus, second-order transfer functions are essentially applied in two steps rather than one, and that simplification alone accounts for most of the improvement in goodness of fit.

Again, the goodness of fit is reasonably good over the middle of the period range for both spatial locations, i.e. the fit is good for those frequencies containing most of the wave energy. As noted in Section 4.3, this increased explanatory power is presumably due to having more energy in the input and output processes at these frequencies for the identification process from which to estimate transfer functions. The long-period low-amplitude waves are presumably 'lost' amongst the higher amplitude waves coinciding with the higher energy content of the wave spectrum.
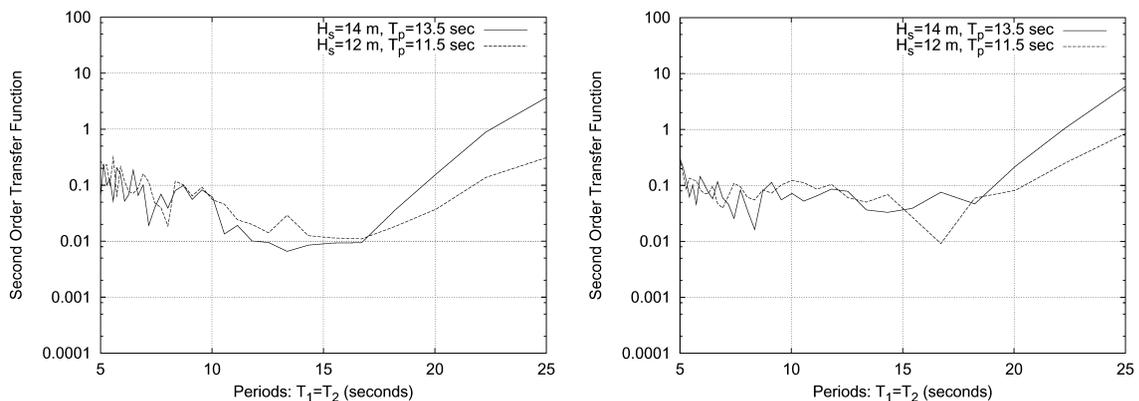

Fig. 12. System ID results: η QTFs; locations 7 (left) and 1 (right): platform center, and in front of first column.
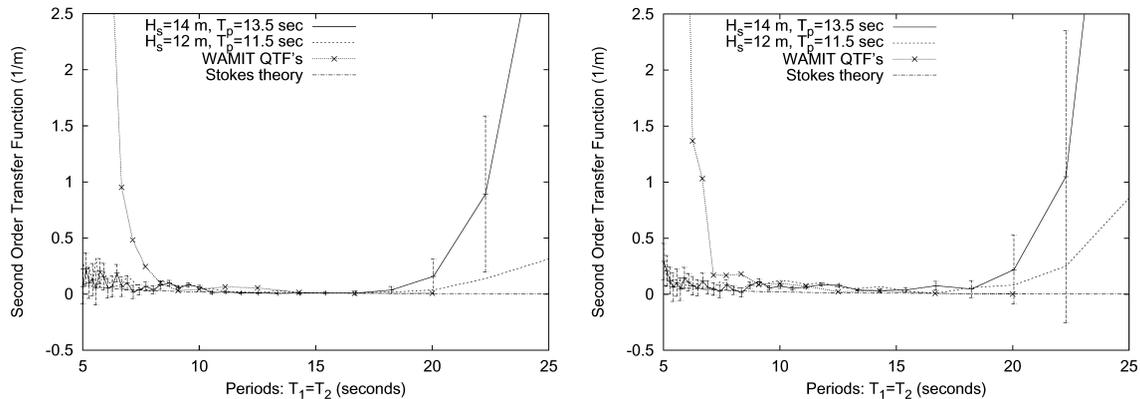
Fig. 13. System ID results: η QTFs; locations 7 (left) and 1 (right): platform center, and in front of first column.

Further evidence for this hypotheses is offered in Fig. 17, where the fraction of power explained can be observed to have a shape comparable to that of a sea-spectrum. Thus, it is suggested that the divergence observed at long-period ranges is not due to any physical phenomenon, but rather is due to lack of long-period data in the time-histories and low amplitudes in those few long-period wave cycles that are available. This phenomenon also occurs in the case of identifying an artificial wave time-history generated by second-order model (Fig. 10).

A more detailed plot of the goodness of fit for the simulated time-history is presented in Fig. 15. The figure shows that, as expected, nearly all of the power is explained by the second-order identification over this frequency range. The simulation and system identification were both performed over the (LTF) frequency range of 0.024–0.34 Hz. Any power identified outside this range is due entirely to quadratic effects. In this figure, the *x*-axis has been converted to frequency rather than period to more clearly show the effects of multiples of frequency expected in a second-order process.

A comparable plot of the goodness of fit for the observed time-history is presented in Fig. 16. Here, the frequency range for the system identification was 0.02–0.20 Hz, which captures most of the energy in the wave spectrum. Again, any power identified outside this range is due entirely to second-order (QTF) effects.

One of the principal goals of this system identification work is to assess the believability of the WAMIT QTFs below about 8 s. The amount of power in observed time-histories, which cannot be explained by a best-fit quadratic transfer function, increases in this interesting period range. On the surface, this observation would seem to suggest that perhaps there are in fact meaningful higher-order effects in the period range below 8 s. Such an observation might increase the level of confidence in these WAMIT transfer functions.

However, a closer examination of the data suggests otherwise. Recall the magnitude of the difference in the two sets of QTF predictions: WAMIT predicts maximum QTFs of about 10, while system identification predicts QTFs of about 0.1. If WAMIT were correct, then nearly all $(1-0.1/10 = 99\%)$ of the power at a 5 s period would be due to the quadratic term not found by the identification analysis, and so there would be substantially more unexplained power due to the incorrectly identified QTF. Thus, a more careful examination shows that the fraction of power explained also supports the idea that the WAMIT transfer function estimates are inaccurate in the short period range.

The most important observation to be made in this section is that over the frequency range of interest, that containing most of the wave energy, the second-order system identification model explains a very large fraction of
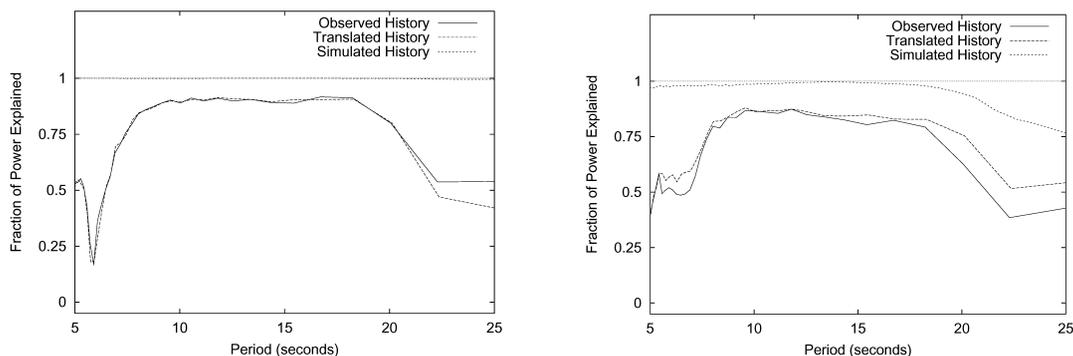

Fig. 14. System ID results: goodness of fit; locations 7 (left) and 1 (right). $H_s = 14.0$ m, $T_p = 13.5$ s.
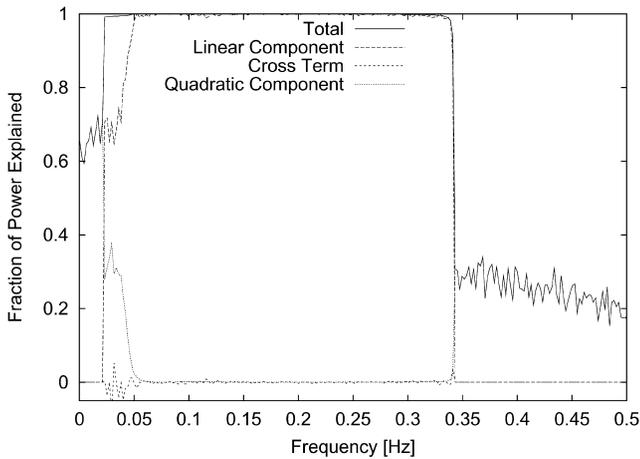
Fig. 15. System ID results: goodness of fit; location 7; simulated wave history. $H_s = 14.0$ m, $T_p = 13.5$ s.

the observed power. The success of the model suggests that most of the energy in the system is due to first- and second-order components, and not due to higher-order terms. This observation suggests that some second-order hydrodynamic model should theoretically be capable of modeling the airgap demand for semi-submersibles. That is, if WAMIT were to be improved to become capable of modeling these effects, the improvement would need to be in the second-order model rather than in addition of, for example, a third-order component to the diffraction analysis.

Teigen and Trulsen [2] obtained supporting results suggesting that the second-order term is far larger than higher-order terms. This conclusion was reached by completely different methods. In that work, two distinctly different methods are employed. One is based on a perturbation expansion method and the other on a fully non-linear hydrodynamic approach. One of their conclusions is that 'the first and second harmonic contributions appear to be the dominant ones, and far more important than those coming from higher-order terms'.
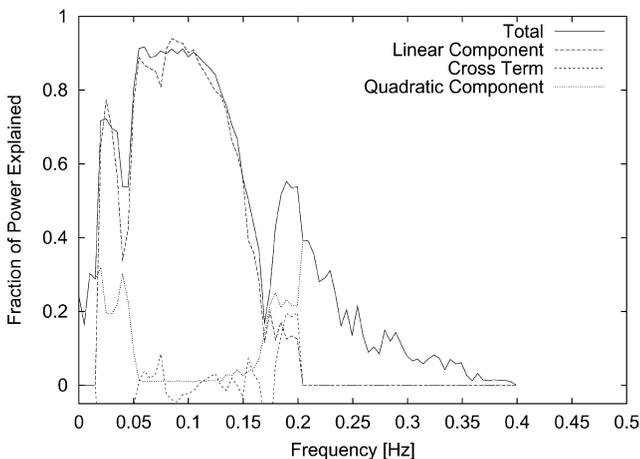

Fig. 16. System ID results: goodness of fit; location 7; measured wave history. $H_s = 14.0$ m, $T_p = 13.5$ s.
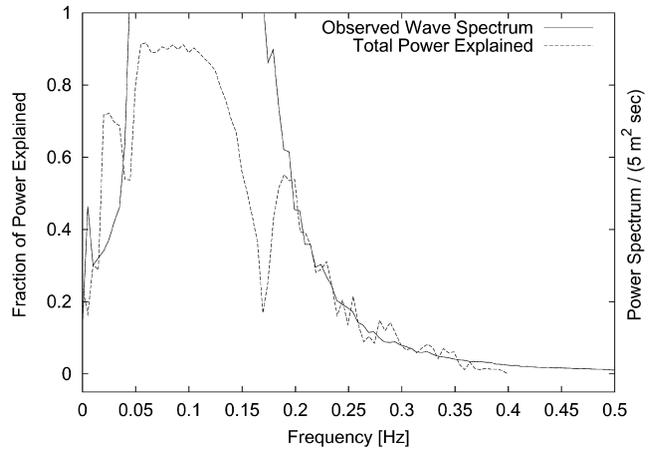

Fig. 17. System ID results: goodness of fit for measured wave history compared with truncated power spectrum of measured wave; location 7. $H_s = 14.0$ m, $T_p = 13.5$ s.

6. Conclusions

System identification of measured model test data has provided additional support for the Stokes substitution proposed in Refs. [5,6].

Identified QTFs agree poorly with those predicted by WAMIT for periods below about 8 s. If WAMIT were correct for this period range, reasonable agreement between WAMIT results and those of system identification should be obtained. This lack of agreement supports the concept of not using the 'suspicious' exponentially growing second-order transfer functions predicted by WAMIT in this period range.

Identified transfer functions below 8 s show better agreement with Stokes than with WAMIT, which supports use of Stokes QTFs rather than WAMIT QTFs in this period range.

Stokes provides a better estimate of these identified transfer functions than does zero. Use of zero is implied by excluding high frequencies from the WAMIT mesh in the original diffraction analysis.

Application of black-box system identification to observed time-histories appears to have been successful. 'reasonable' LTFs and QTFs have been obtained. All of the significant trends observed in the system identification results appear justifiable.

The hypothesis proposed in Section 4 is incorrect. The hypothesis was that one possible explanation for the seemingly large QTFs predicted by WAMIT is that these QTFs are in fact correct to second-order; and that the problem lies in the second-order assumption. It was hypothesized that inclusion of higher-order terms (e.g. third, fourth, etc.) would have an offsetting effect, resulting in prediction of a total process which agrees well with observed data.

The amount of power in observed time-histories which cannot be explained by a best-fit quadratic transfer function is very small compared with that implied by the QTFs

predicted by WAMIT below 8 s. If the true second-order transfer functions were in fact near to the WAMIT estimate, then the much smaller QTFs obtained from identification would be capable of explaining only a minute fraction (e.g. 2% in a worst case) of the power observed in the very low period range.

References

[1] Winterstein SR, Sweetman B. Air gap response of floating structures: statistical predictions vs observed behavior. ASME J Offshore Mech Arctic Engng 2001;123:118–23.

[2] Teigen P, Trulsen K. Numerical investigation of non-linear wave effects around multiple cylinders. Proceedings of the International Offshore Polar Engineering, ISOPE; 2001. p. 369–78.

[3] Manuel L, Sweetman B, Winterstein SR. Analytical predictions of the air gap response of floating structures. J Offshore Mech Arctic Engng 2001;123:112–7.

[4] Manuel L, Winterstein SR. Reliability based predictions of a design air gap for floating offshore structures. Proceedings of the Eighth ASCE Conference on Probabilistic Mechanics and Structural Reliability, ASCE; 2000.

[5] Sweetman B, Winterstein SR, Meling TS, Birknes J. Airgap prediction: use of second-order diffraction and multicolumn models. Proceedings, ISOPE 2001-IL-13, ISOPE; 2001. available from www.rms-group.org.

[6] Sweetman B, Winterstein SR, Meling TS. Airgap prediction from second-order diffraction and stokes theory. Int J Offshore Polar Engng 2002;12(3).

[7] WAMIT 5.3. WAMIT: user manual versions 5.4, 5.4PC, 5.3S, Department of Ocean Engineering, MIT; 1999.

[8] Fokk T. VeslefrikkB air gap model tests. Technical report 512167.00.01, Trondheim, Norway: MARINTEK; 1995.

[9] Kac M, Siegert AJF. On the theory of noise in radio receivers with square law detectors. J Appl Phys 1947;(18):383–400.

[10] Næss A. The statistical distribution of second-order slowly varying forces and motions. Appl Ocean Res 1986;8:110–8.

[11] Næss A. Prediction of extremes related to the second-order, sum-frequency response of a tlp. Proceedings of the Second International Offshore Polar Engineering, ISOPE; 1992. p. 436–43.

[12] Winterstein SR, Ude TC, Marthinsen T. Volterra models of ocean structures: extreme and fatigue reliability. J Engng Mech 1994; 120(6):1369–85.

[13] Crandall SH, Mark WD. Random vibration in mechanical systems, monograph. New York: Academic Press; 1963.

[14] Winterstein S. Nonlinear vibration models for extremes and fatigue. J Engng Mech, ASCE 1988;114(10):1772–90.

[15] Ude TC. Second-order load and response models for floating structures: probabilistic analysis and system identification. Technical report RMS-16. Reliability of marine structures, Department of Civil Engineering, Stanford University; 1994.

[16] Winterstein SR, Sweetman B, Jha A. Spatial prediction of non-linear random ocean waves: identification of Gaussian and non-Gaussian contributions. Proceedings, PMC-2000-340, ASCE; 2000.

[17] Sweetman B, Winterstein S. Second-order random ocean waves: prediction of temporal and spatial variation from fixed and moving references. Technical report RMS-37. Reliability of Marine Structures; 1999.